Int J Adv Manuf Technol
DOI 10.1007/s00170-015-7870-z

ORIGINAL ARTICLE

Principles and applications of trans-wafer processing using a 2-μm thulium fiber laser

Ilya Mingareev[1,2] · **Nils Gehlich**[1,2] · **Tobias Bonhoff**[1,2] · **Ali Abdulfattah**[1] · **Alex M. Sincore**[1] · **Pankaj Kadwani**[1] · **Lawrence Shah**[1] · **Martin Richardson**[1]

Received: 9 July 2015 / Accepted: 15 September 2015
© Springer-Verlag London 2015

Abstract A self-developed nanosecond-pulsed thulium fiber laser operating at the wavelength λ=2 μm was used to selectively modify the front and the back surfaces of various uncoated and metal-coated silicon and gallium arsenide wafers utilizing transparency of semiconductors at this wavelength. This novel processing regime was studied in terms of the process parameter variations, i.e., pulse energy and pulse duration, and the corresponding modification fluence thresholds were determined. The results revealed nearly debris-free back surface processing of wafers, in which modifications could be induced without affecting the front surfaces. The back surface modification threshold of Si was significantly higher than at the front surface due to non-linear absorption and aberration effects observed in experiments. A qualitative study of the underlying physical mechanisms responsible for material modification was performed, including basic analytical modeling and z-scan measurements. Multi-photon absorption, surface-enhanced absorption at nano- and microscopic defect sites, and damage accumulation effects are considered the main physical mechanisms accountable for consistent surface modifications. Applications of trans-wafer processing in removal of thin single- and multi-material layers from the back surface of Si wafers, both in single tracks and large areas, are presented.

Keywords Infrared lasers · Laser materials processing · Semiconductors

1 Introduction

Over the last two decades, pulsed laser processing of semiconductor wafers has proven a very active and important field of research attracting immense academic and practical interest. Various processing regimes have been extensively studied, e.g., for laser-induced wafer singulation and surface functionalization [1–4], annealing, film deposition, and ion implantation [5–9]. In particular, investigations of wafer surface damage mechanisms caused by the interaction of high-intensity laser light with silicon and gallium arsenide have been of great significance for semiconductor industry [3–5, 10–15], due to the widespread use of these materials in microelectronics and photonics applications. Yet, further advancements in wafer processing technologies are required to enable fabrication of next-generation, high-performance electronic, and photonic devices.

A large number of theoretical, numerical, and experimental studies have been already devoted to investigations of laser-semiconductor interaction mechanisms and surface modifications using laser sources operating in the spectral range from ultraviolet to near-infrared. However, following the recent advancements in the development of novel continuous wave and pulsed near-infrared (near-IR) and mid-infrared (mid-IR) lasers, a new processing regime for semiconductors was recently established that utilizes photon energies smaller than the semiconductor's energy band gap E_g. In particular, formation of sub-surface modifications in semiconductors was studied to enable "stealth dicing" by inducing a belt-shaped polycrystalline layer in the bulk of silicon wafers and using near-IR laser radiation [1, 2]. In-volume modifications in silicon wafers

✉ Ilya Mingareev
mingareev@ucf.edu

[1] Townes Laser Institute, CREOL, College of Optics and Photonics, University of Central Florida, Orlando, FL 32816, USA

[2] Fraunhofer Institute for Laser Technology, Aachen 52074, Germany

Published online: 03 October 2015

were achieved using tightly focused pulsed laser radiation at the wavelength 1.55 μm and sub-picosecond pulse duration [16]. Inscription of optical waveguides in the proximity of the silicon/silicon oxide interface was reported using mid-IR femtosecond laser pulses [17]. Finally, internal modifications in silicon presumably resulting from two-photon absorption were achieved using nanosecond laser pulses at the wavelength 1.55 μm [18]. For this new processing regime, the mechanisms of light absorption and energy transfer leading to material modifications, in particular, in the bulk of semiconductors, need to be reevaluated. In addition, process conditions and limitations need to be studied to enable new applications such as layer-selective processing or in-volume scribing.

In this work, experimental studies on laser processing of silicon and gallium arsenide with nanosecond laser pulses produced by a thulium-doped photonic crystal fiber (PCF) master oscillator power amplifier (MOPA) system at the wavelength λ=2 μm ($\hbar\omega\approx$0.62 eV) are presented. Pulsed Tm/fiber laser systems have already proven to be well suited for light detection and ranging (LIDAR) applications, and for pumping of mid-IR optical parametric oscillators (OPO). Such applications require relatively high peak power pulses and nearly diffraction-limited beam quality with linear polarization. Therefore, it is highly advantageous to use fibers that offer the largest possible mode area while maintaining fundamental mode propagation. Previously, it has been shown that thulium-doped PCFs provide mode areas >1000 μm^2 [19] and yield nearly perfect beam quality and polarization and that these fibers are well suited for use in high peak power Q-switched oscillators [20, 21]. In the record demonstration to date, PCFs have been used to scale peak powers towards the megawatt level in thulium-based MOPA systems [22].

In this study, it was shown that by utilizing semiconductors' transparency at λ=2 μm, modifications can be induced not only at the front (laser incident) surface but also at the back surface of thin wafers. An experimental validation was provided that the back surface of Si and GaAs wafers could be modified independently, without inducing damage to the front surface. Therefore, this approach is referred to as the trans-wafer processing. The influence of process conditions on the resulting surface morphology change was studied by varying incident pulse energy and laser pulse duration. The laser-induced surface modifications were investigated by optical microscopy and scanning electron microscopy (SEM), and the modification thresholds for multiple-pulse irradiation were estimated for front and back surfaces. Basic z-scan transmission measurements were performed to evaluate the contribution of multi-photon absorption (MPA) mechanisms to processing of semiconductors at the wavelength λ=2 μm. In addition, trans-wafer processing was applied to space-selectively remove different metallization coatings from the back surface of Si wafers.

2 Experimental details

2.1 Laser system

The first amplifier stage of the self-developed MOPA system described in [22] was used for the semiconductor irradiation experiments in this study. The maximum peak power was >40 kW, with approx. 400 μJ maximum pulse energy at 6.8 ns and 1 kHz repetition rate. The output was linearly polarized, the initial beam diameter was approx. 4.5 mm, the beam quality was M^2<1.2, and the spectral width was <1 nm (full width at half maximum, FWHM) at the wavelength 1985 nm. The pulse duration was adjustable in the range t_p= 6.8–100 ns. The spectral, temporal, and spatial characteristics of the laser radiation (Fig. 1) produced by the MOPA system were monitored for different levels of pulse energies, and no significant variations of the spatial beam profile with regard to its shape and size were determined within the range of process conditions adopted in the experiments.

2.2 Utilized semiconductor materials

For basic studies of front and back surface modifications, uncoated intrinsic double-side polished semiconductor wafers were used. The Si wafers (Cz-Si, Virginia Semiconductor)

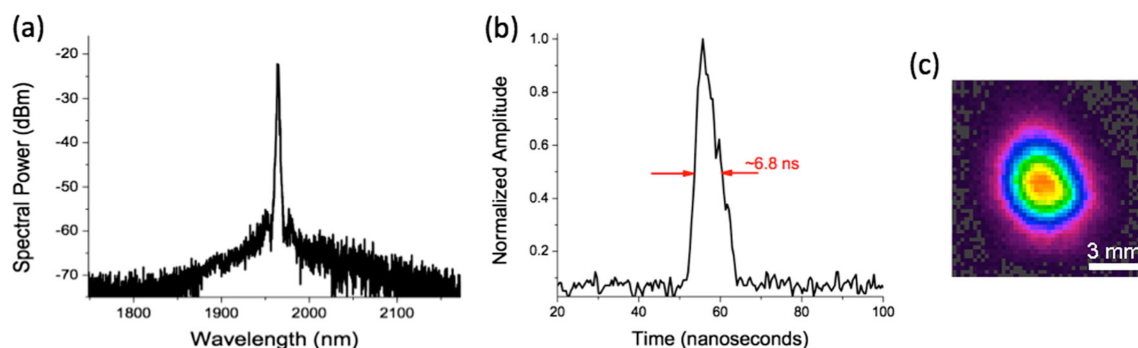

Fig. 1 **a** Output spectrum of the Tm-fiber MOPA system, **b** temporal pulse profile, **c** spatial output beam profile

had a thickness of 500 μm with the normal axis along the [110] crystal direction, and the GaAs wafers (Wafer World) were 600 μm thick with the normal axis along the [100] crystal direction. For coating removal studies, four different material systems (ML 1–4) were used with either a single metallization layer or a complex multi-layer composition. The coatings were produced using commercial sputter coating and plasma-enhanced chemical vapor deposition (PECVD) equipment. The material compositions of the coatings are presented in Table 1.

Material interfaces such as Ti/TiN and Ti/NiV deposited on Si are widely used as metallization layers in many current and prospective photovoltaic module designs. Substrates used in samples ML 1 and ML 2 were intrinsic double-side polished Si wafers, whereas samples ML 3 and ML 4 were based on 180 μm p-Si substrates that were wet-etched to reveal a random pyramid texture as commonly used in photovoltaic applications. The base resistivity of p-doped substrates was 4 Ω cm.

2.3 Irradiation procedures and material characterization

As shown in Fig. 2, the output of the MOPA system was directed through a mechanical shutter (Uniblitz) in order to control the number of pulses incident on the target. The beam was then directed along a vertical rail to achieve normal incidence of the beam onto the horizontally mounted targets. The beam was focused to an approx. 10-μm spot size using an aspheric lens with a focal length f=7.5 mm. Refraction properties of semiconductors were taken into account when determining the focus position at the back surfaces of the samples (refractive indices n_{Si}=3.45 and n_{GaAs}=3.36 at λ=2 μm). Sequential ray-tracing modeling using Zemax was carried out to simulate the intensity distribution and the focus position at the back surface by taking into account linear refraction and aberration effects. The wafer targets were mounted on a 3-axis motion controller stage (Newport VP-25X), while the lens was stationary. Co-axial imaging arrangement comprising a CMOS camera and a 1.25× imaging objective was adopted to monitor back surface modifications.

The repetition rate was set to f_{rep}=1 kHz for all basic surface modification experiments. Irradiations were performed at pulse energies E_p<350 μJ and at two pulse durations t_p=7 ns and t_p=100 ns. Unless stated otherwise, trenches were produced by translating the sample in the focal x-y plane at a constant speed v=1 mm/s orthogonally to the incident laser beam. Alternatively, irradiation with a specified number of laser pulses carried out at fixed positions produced surface craters. For the coating removal experiments, the repetition rate was set to f_{rep}=20 kHz and the samples were translated at the speeds v=1–2 mm/s.

Basic open-aperture z-scan method was adopted to study the non-linear response of intrinsic Si and GaAs samples. For this experiment, laser radiation was focused using an f= 25 mm aspheric lens. Surface resistance of laser-processed coated samples was measured using the 4-terminal method with a Hewlett-Packard 3456A digital multimeter.

Surface modifications were analyzed by optical microscopy (Olympus BX51) and scanning electron microscopy (Zeiss Ultra 55 and JEOL JSM-6480). Energy-dispersive X-ray spectroscopy (EDX) was utilized to investigate the elemental composition of the laser-produced debris. Processed samples were not cleaned before surface characterization in order to examine the morphology, amount, and composition of process-induced debris.

3 Processing of uncoated semiconductor surfaces

Experimental conditions and the resulting surface morphology modifications were investigated both for the front and the back surface processing of the samples. In the first series of experiments, the laser radiation was focused on the front surface of the samples (z_0 position) to study the resulting morphology change by translating the sample and at fixed points, in dependence on the laser pulse energy and the pulse duration.

The morphology of craters produced in Si and GaAs with 1000 pulses at 7 and 100 ns pulse duration revealed differences in material response to laser irradiation (Fig. 3). Depending on the pulse duration, as the material undergoes melting and sublimation, its products are ejected and re-solidified at the surface differently. In case of Si, the material removal process was accompanied with the dispersion of micrometer-sized, mostly spherically shaped debris particles to a wide surface area for t_p=7 ns. For t_p=100 ns pulses, the area

Table 1 Material composition of multi-layer coated semiconductor samples

Notation	Substrate	Coating composition	Coating deposition method
ML 1	Intrinsic Si (1 mm)	Ni (100 nm)	Sputter coat
ML 2	Intrinsic Si (500 μm)	Ti (70 nm)	PECVD
ML 3	p-Si (180 μm)	SiO_2 (500 nm), TiN (100 nm), Ti (20 nm)	PECVD
ML 4	p-Si (180 μm)	SiO_2 (1500 nm), Ti (100 nm), NiV (200 nm), Ti (20 nm)	PECVD

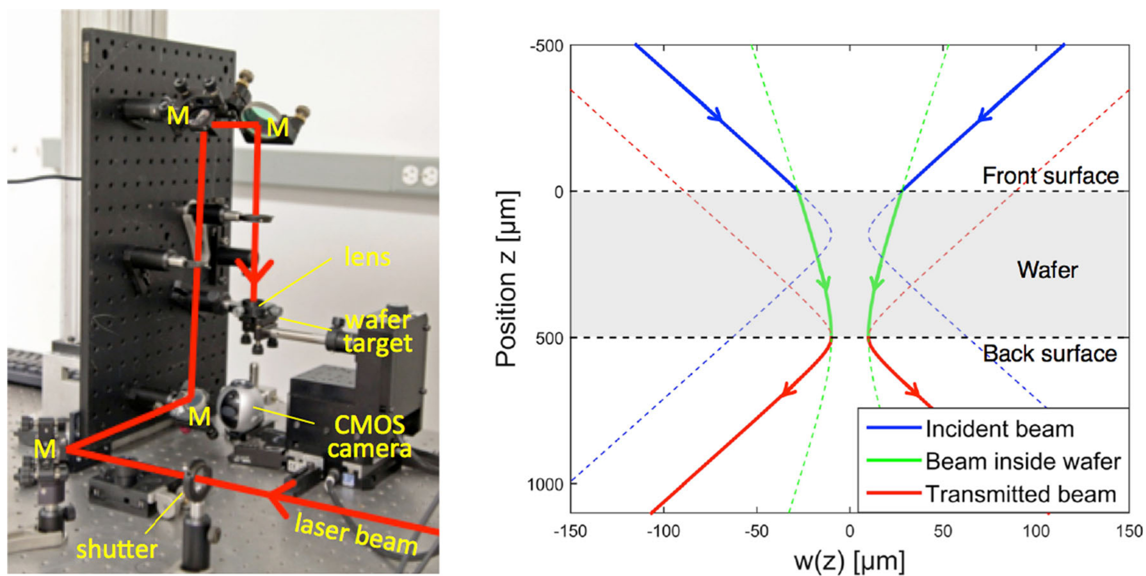

Fig. 2 *Left*: Trans-wafer irradiation setup (*M*—mirrors). *Right*: Model of a beam caustic for optical propagation through a semiconductor wafer in air, with the incident Gaussian laser beam (*solid blue line*) coming from top, beam propagation inside the wafer (*solid green line*) and transmitted beam (*solid red line*). *Dashed lines* indicate no-refraction portions of the corresponding beam caustics

surrounding the craters was covered with up to approx. 60 μm long, radially distributed re-solidified material "splatter" originating from the craters. Ring-like surface swellings were observed around the craters, probably resulting from the periodical melting and re-solidification process and indicating a larger contribution of thermal phenomena during irradiation with longer laser pulses. When the same experimental conditions were applied for processing of GaAs samples, a larger amount of debris was generated compared to Si. A large round area around the craters was splash coated with ablation products. EDX measurements indicated up to 18 wt% of oxygen in close vicinity (≈10 μm) of craters, with the oxygen fraction vanishing with increasing distance from the craters. The debris film appeared cracked and also exposed sites where the debris stripped off the wafer surface. These sites did not seem to be significantly heat affected, showing extremely smooth surface quality and approx. 0.5 wt% of oxygen according to the EDX analysis similar to the unprocessed bulk material. Irradiation

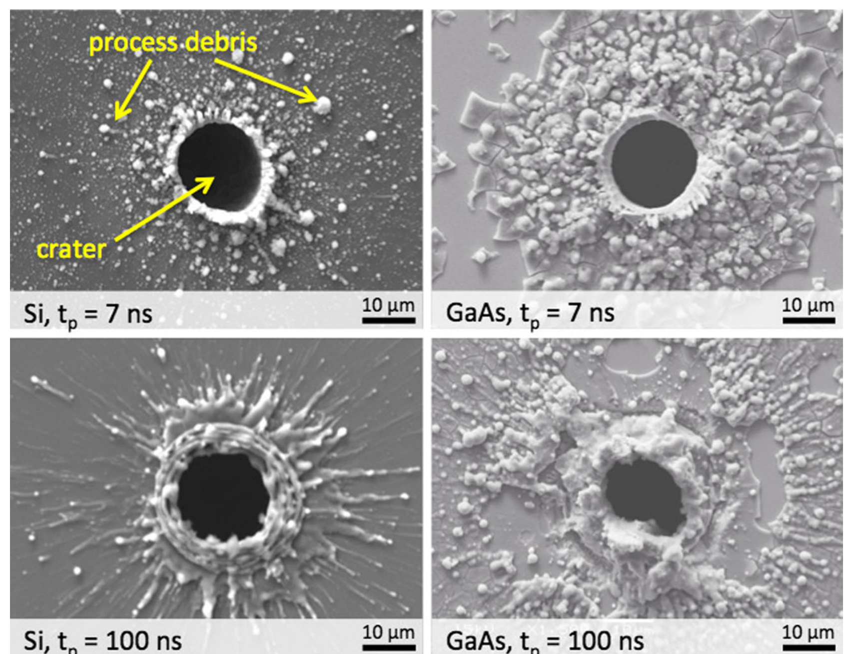

Fig. 3 SEM images of front surface craters produced in Si and GaAs utilizing 1000 pulses at E_p=120 μJ

of GaAs with t_p=100 ns pulses produced an excessive amount of recast material.

Trenches were produced on the front surface of Si and GaAs samples by applying the same experimental conditions as for the irradiation at fixed positions and by translating the samples in the *x-y* plane at a constant speed v=1 mm/s resulting in a spatial pulse overlap of approx. 90 %. The trenches obtained in Si (Fig. 4, left) at t_p=7 ns were surrounded by a large amount of melted and re-solidified material and individual micrometer-sized melt droplets dispersed on the surface. Interestingly, Si trenches produced at t_p= 100 ns (Fig. 4, middle) did not reveal a deep modification as compared to irradiation with shorter pulses. Instead, a more confined region with a smaller width and featuring apparently melted and re-solidified material was detected. Similar to irradiation at fixed surface positions, processing of trenches in GaAs (Fig. 4, right) produced a continuous debris film as well as sporadic splashes of re-solidified material.

In the second series of experiments, transparency of semiconductors at the wavelength λ=2 μm was utilized to induce surface modifications at the back surface. When a focused laser beam passes through a Si or a GaAs wafer, it is subject to considerable refraction and Fresnel reflections from both surfaces. In general, these effects can significantly affect focusing conditions at the back surface due to spherical aberrations and multiple reflections of the beam inside the wafer. In addition, semiconductors exposed to high-intensity electromagnetic fields are subject to non-linear optical effects, such as absorption, beam focusing/defocusing, and scattering. Therefore, irradiation conditions at the back surface cannot be compared to front surface irradiation directly.

To achieve back surface modifications, the wafer was first translated approximately Δz=1 mm along the *z*-axis towards the focusing lens. This procedure ensured the initial laser focus was well below the back surface of the wafer. Afterwards, the distance between the assumed focus position and the back surface was gradually reduced while concurrently translating the wafer in the *x-y* plane at 1 mm/s to produce trenches. Irradiations were performed at different pulse energies to determine the threshold value for the processing initiation. The onset of the back surface modification in GaAs (Fig. 5, right) was observed at a position offset $\Delta z \approx 210 \pm 20$ μm measured from the initial z_0 position, which roughly corresponds to the focus being at the back surface according to the simulation data for the 600-μm-thick wafer. The modification morphology revealed trenches apparently induced by a thermal melting process, predominantly. Compared to modifications achieved at the front surface, the areas surrounding the trenches were covered with a notably reduced amount of debris. Surface analysis by optical microscopy and SEM indicated no evidence of modification at the corresponding sites of the front surface in GaAs at pulse energies adopted. It should be noted that back surface modifications were only possible when producing trenches, as single-spot irradiations did not consistently result in reproducible ablation crater generation.

Back surface irradiation of Si (Fig. 5, left) was carried out utilizing the same procedure as for GaAs. Following the same geometric considerations and taking into account possible spherical aberrations and the optical path length in a 500-μm-thick Si wafer, the wafer position offset corresponding to the beam focus being at the back surface was estimated to $\Delta z \approx 180 \pm 20$ μm using the ray-tracing model produced by Zemax. However, in experiments, processing of Si at pulse energies comparable to those adopted for GaAs did not result in any detectable back surface modification and only the front surface could be modified with increasing pulse energy and/or decreasing Δz. By replicating the experiment while gradually increasing the pulse energy, the onset of the back surface modification was observed at a much larger offset of $\Delta z \approx$ 450 μm than predicted by simulations. The resulting surface morphology represented trenches produced presumably by local surface re-melting process; however, no evidence of debris generation was detected. Similar to GaAs, no visible damage was induced to the front surface of Si at these experimental conditions. While back surface modifications at a larger *z*-offset can be explained by higher intensities throughout the

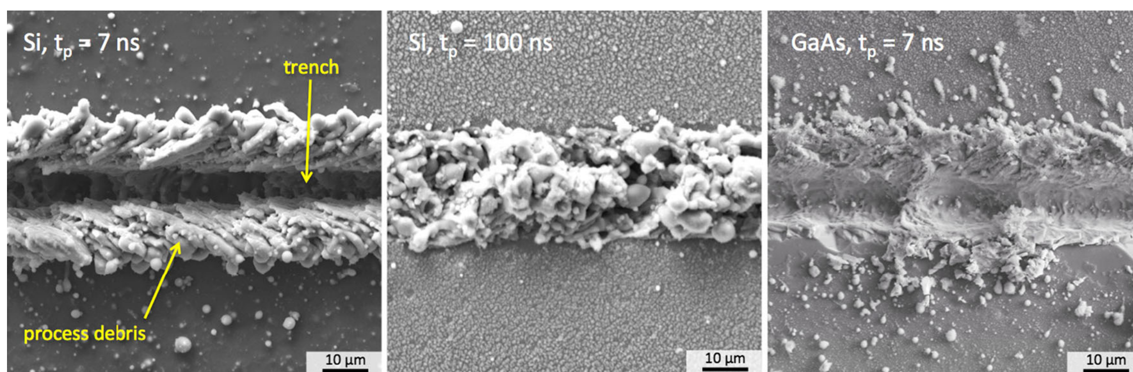

Fig. 4 SEM images of front surface trenches induced at v=1 mm/s. Si processed at E_p=145 μJ, t_p=7 ns (*left*) and t_p=100 ns (*middle*). GaAs processed at E_p=120 μJ and t_p=7 ns (*right*)

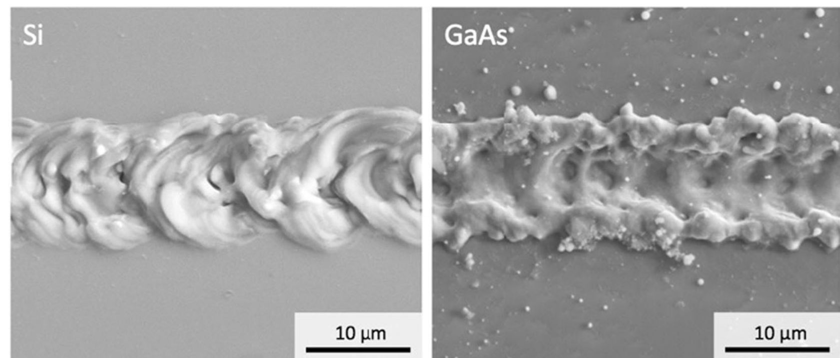

Fig. 5 SEM images of back surface modifications induced at t_p=7 ns, v=1 mm/s. *Left*: Si processed at E_p=320 µJ, *right*: GaAs processed at E_p=120 µJ

beam path, the lack of modifications at the geometrically estimated focus position around $\Delta z \approx 180$ is an indication of a complex spatial energy distribution in the laser-material interaction zone caused by non-linear material response.

Similar to irradiation of front surfaces, a different modification behavior was observed for the irradiation of back surfaces of Si wafers using longer laser pulses (Fig. 6). While no deep modifications were detected both for 7 and 100 ns laser pulses, the morphology of the laser-induced surface change obtained with longer pulses revealed a larger contribution of thermal phenomena to the modification process. In case of irradiation with 100 ns laser pulses, periodic re-solidified pattern was observed, with a period of approx. 1 µm, and apparently resulting from overlapping single-pulse modifications.

4 Determination of modification thresholds

To determine the energy density thresholds for the front surface modifications, surface craters were produced by applying 20 pulses at varying pulse energies E_p=10–150 µJ. After irradiation, the diameters d of the craters were determined by optical microscopy. Using this experimental data and the model from [23],

$$d^2 = 2w_0^2 \ln\left(E_p/E_{p,th}\right) 2w_0^2 \ln(F/F_{th}) \quad (1)$$

the beam waist size w_0 and the modification fluence threshold F_{th} can be determined by performing a linear regression of d^2 as a function of ln E_p. Evaluation of the experimental data resulted in the beam waist w_0=10 µm in all measurements performed at the front surface. The fluence threshold data for the pulse durations 7 and 100 ns is summarized in Table 2.

Irradiations performed with a smaller number of pulses did not deliver consistent results, which was caused by considerable discrepancies in the crater diameters obtained. However, the experiment confirmed that the fluence threshold values were in general larger with the smaller numbers of pulses (<20) applied. Similar behavior and dependency of the threshold values on the number of pulses were reported for nanosecond laser processing of semiconductors at other wavelengths [15, 24].

A reliable determination of the back surface modification thresholds was not possible by measuring the crater diameters due to mainly probabilistic nature of their generation and large discrepancies in their diameters. The experiments showed that only wafer processing by translating the samples in the x-y

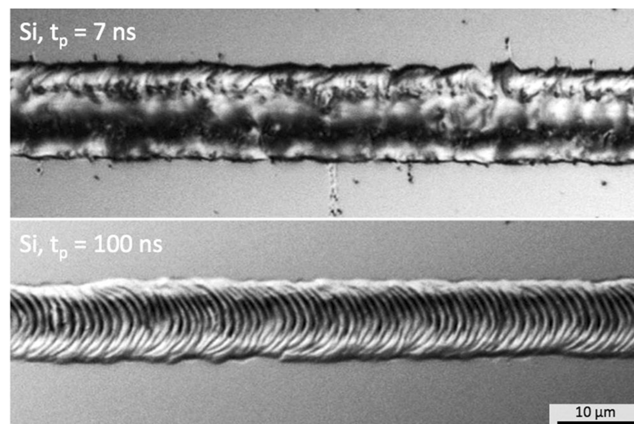

Fig. 6 Optical microscopy images of back surface modifications obtained in Si at v=1 mm/s, E_p=294 µJ, and different pulse durations

Table 2 Front and back surface modification thresholds for Si and GaAs at λ=2 µm

Material	Pulse duration [ns]	Front surface fluence threshold[a] [J/cm^2]	Back surface fluence threshold[b] [J/cm^2]
Si	7	2.86	<17.2
	100	3.22	
GaAs	7	2.30	<3.2
	100	3.38	

[a] Determined for craters produced with 20 pulses

[b] Estimated for trenches with 10 effectively incident pulses

plane resulted in consistent modifications induced at the back surface. In addition, while performing such experiments, occasional modifications were observed that apparently originated from laser beam interaction with microscopic irregularities of the wafer surface, e.g., micro-craters and scratches. This "initiation effect" implies damage accumulation phenomena could play an important role in the physical mechanism of back surface processing. Therefore, based on the experimental results obtained, only an upper limit estimation of the modification thresholds could be provided.

The minimum pulse energy necessary to induce back surface trenches in GaAs was E_p=18 μJ. Without an exact knowledge of light propagation and absorption conditions in the bulk, it was impossible to determine what fraction of the incident optical energy was effectively contributing to the back surface modification process. Thus, the only measurable parameter was the transmittance T_{GaAs}=54.6 % through the entire wafer. Assuming the laser beam waist of w_0=10 μm as resulted from ray-tracing modeling, taking into account the wafer transmittance, and considering the accumulated energy applied to a single spot being equivalent to 10 pulses, the corresponding fluence threshold was estimated to F_{th}<3.2 J/cm^2 for 10 pulses at t_p=7 ns.

For Si, the minimum pulse energy required for consistent back surface modification was E_p≈100 μJ; however, sporadic modifications were also possible at lower pulse energies. With the total wafer transmittance T_{Si}= 53.4 % and the offset Δz corresponding to the processing initiation being much larger than predicted by ray tracing modeling, only a rough estimation for the modification threshold can be given. Accordingly, the back surface modification threshold for Si is F_{th}<17.2 J/cm^2 for 10 pulses with the pulse duration t_p=7 ns.

While the utilized threshold determination method itself is not sensitive to uncertainties resulting from the beam size characterization as long as the spatial beam profile is nearly Gaussian, its accuracy depends critically on the measurement uncertainty of the laser-induced crater diameters. Therefore, surface damage that is not detectable by optical microscopy or SEM could increase the measurement errors. Taking into account the calibration uncertainty of pulse energy measurements in the experimental series presented here, the errors were estimated to be within ±6 and ±15 %, for all front and back surface fluence threshold measurements, respectively. A higher uncertainty in back surface threshold data resulted from larger measurement discrepancies of laser-induced back surface features, because more irregular surface structures were developed (Fig. 5). Another potential source of measurement errors is the possible effect of the destructive sample preparation method, e.g., wafer grinding and polishing, which might induce additional damage and is difficult to quantify.

5 Study of possible modification mechanisms

For a conclusive evaluation of the experimental results obtained at the wavelength 2 μm, it is essential to review the underlying physical mechanisms responsible for semiconductor processing. In particular, similarities and differences to processing in the non-transparent regime, i.e., with photon energies $\hbar\omega > E_g$, need to be highlighted. On the one hand, the front surface modification thresholds for Si and GaAs were similar to the values obtained for processing at shorter wavelengths. For example, F_{th}=4.8 J/cm^2 was reported for single-pulse irradiation with 20 ns pulses at λ=1.064 μm [10]. Values in the range F_{th}=2.5–3.8 J/cm^2 were reported for differently doped Si, and a wide range of threshold values F_{th}=0.5–3.8 J/cm^2 was reported for GaAs irradiated with nanosecond pulses at different wavelengths [11–15]. On the other hand, irradiation of pure semiconductors with photon energies $\hbar\omega < E_g$ enabled a new, different processing regime which allowed a spatially selective modification of the wafers' back surfaces. This implies significant differences in the underlying modification mechanisms and principles.

5.1 Absorption of mid-IR laser radiation

In general, laser-semiconductor interaction utilizing high-intensity laser pulses with photon energies $\hbar\omega > E_g$ reveals three primary absorption mechanisms. First, intrinsic absorption is caused by interband electronic transitions. Free carrier absorption is the second important mechanism that involves photo-induced intraband transitions followed by the energy transfer to the lattice. The third absorption mechanism, which is characteristic for impure and contaminated materials, is initiated by defects and impurities leading to a lowered energy band gap. Multi-photon absorption is usually not considered an important absorption mechanism for semiconductor processing with $\hbar\omega > E_g$, because material modifications such as melting and ablation occur at much lower intensities than needed for multi-photon absorption to become predominant.

In contrast, for photon energies $\hbar\omega < E_g$ and pure semiconductors, intrinsic absorption vanishes and free carrier absorption becomes negligible. Therefore, the effects of multi-photon absorption on material processing require further considerations involving energy budget analysis for different experimental conditions. In addition, electron avalanche ionization is an important, secondary non-linear carrier excitation mechanism that however requires background (seed) electrons generated by aforementioned absorption processes. Therefore, knowledge of the origin and the density of photo-excited seed electrons is essential for the evaluation of the material modification processes for different photon energies.

Following a simple, first-principles model describing laser heating of semiconductor surfaces and their thermomechanical behavior [25], the temperature rise of a

material irradiated at a fluence F can be estimated. If the optical energy is added to the material uniformly within the heating depth L_H, the temperature rise ΔT can be expressed as

$$\Delta T = \frac{F(1-R)}{pcL_H}, \quad (2)$$

where R is the reflectivity, c is the specific heat of the material, and ρ is the mass density. In general, the heating depth L_H can be expressed by the following approximation:

$$L_H \approx \frac{1}{\alpha} + L_D + L_T, \quad (3)$$

where L_D is the carrier diffusion length and L_T is the thermal diffusion length. The total absorption coefficient α can be expressed as a sum of α_{SP}, α_{MP}, and α_{FC} representing single-photon, multi-photon, and free carrier absorption coefficients, respectively. At λ=2 μm, intrinsic absorption is not present and the free carrier absorption is negligible, α_{FC}< <1 cm^{-1} for materials under investigation. Accordingly, multi-photon absorption is considered the only primary absorption process supplying seed electrons for avalanche ionization and subsequent lattice heating. L_D is dependent on the carrier lifetime and the material temperature and considered to be on the order of 1 μm or smaller for Si and GaAs irradiated with nanosecond pulses. For 7 ns pulses, the thermal diffusion depth $L_T \sim t_p^{1/2}$ is negligibly small as well. Therefore, assuming no other primary photoionization processes are involved in semiconductor laser processing at λ=2 μm, Eq. (3) can be simplified to $L_H \approx \alpha^{-1} \approx \alpha_{MP}^{-1}$.

In these experiments, the multi-photon absorption phenomena possibly involved in laser-semiconductor interaction are the two-photon absorption in Si with the 2PA coefficient $\beta_{Si} \approx$ 0.25 cm/GW [26] and the three-photon absorption in GaAs with the 3PA coefficient $\gamma_{GaAs} \approx 0.18$ cm^3/GW^2 [27]. By calculating α_{MP} for both materials, and using the experimentally obtained modification threshold values (Table 2) in Eq. (2), the corresponding temperature rise induced by a single laser pulse would be on the order of only 1 K. In fact, in order to increase the surface temperature to the melting point, a total absorption coefficient on the order of $\alpha \sim 10^3$–10^4 cm^{-1} would be required. Therefore, the contribution of the multi-photon absorption processes to the material modification is very small but not negligible as it can still provide seed electrons for avalanche ionization.

5.2 Measurements of the non-linear material response

In order to evaluate these generalized considerations qualitatively, basic open-aperture z-scan measurements were performed with Si and GaAs wafers. The z-scan technique allows studying non-linear optical properties of transparent materials. A triplet lens (f=25 mm) was used for beam focusing. The repetition was set to f_{rep}=10 kHz rate, and the pulse duration was set to t_p=100 ns, to reduce the risks of wafer damage and to provide sufficient laser power for reliable measurements. Transmission through the wafers was determined as a function of the position z and the pulse energy E_p. Measurements were repeated 5 times, and the wafers were translated in the x-y plane before each new measurement to avoid possible interferences from previous exposures. The combined systematic errors in all transmission measurements were estimated to be below 1 %. The results of the z-scan measurements (Fig. 7) revealed a transmission drop for both materials as the focused beam passed through the wafer. In Si, the transmission decreased from 53.4 % to approx. 41 % for $E_p \leq 25$ μJ, and this dependency was in general non-linear. In GaAs, the transmission decrease was only about 1–2 %, being nearly constant for pulse energies in the range $E_p \leq 24.5$ μJ. However, at $E_p \geq 25$ μJ, a dramatic decrease in transmission was observed, presumably indicating the initiation of wafer modification processes.

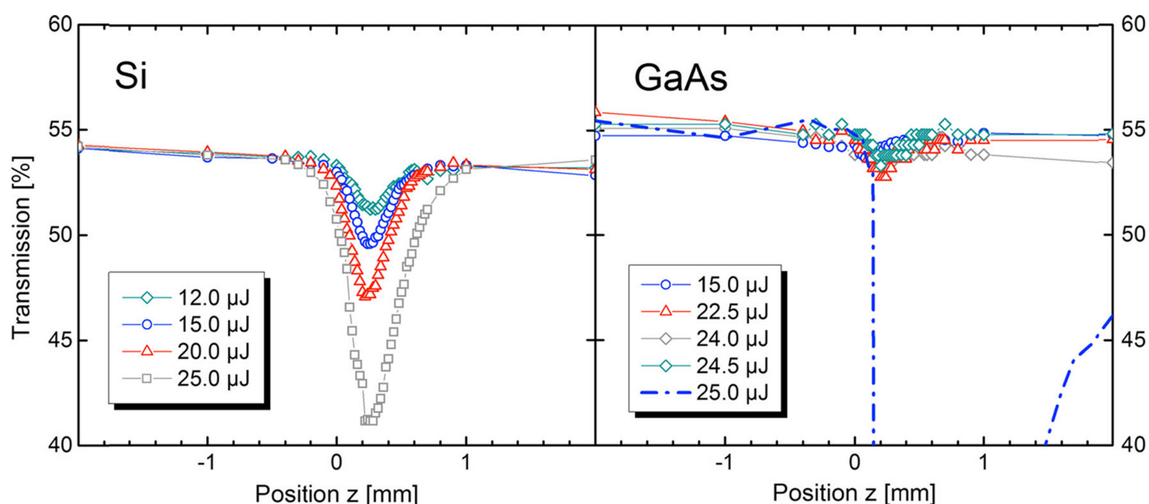

Fig. 7 Results of the open-aperture z-scan measurements. Negative z values represent laser focus being below the wafer

From the results of the z-scan measurements, it can be concluded that two-photon absorption can play a significant role in the modification mechanism of Si, whereas three-photon absorption in GaAs does not appear to contribute to the material modification significantly. Therefore, an alternative absorption mechanism responsible for the generation of a sufficient seed electron density must be assumed.

5.3 Alternative surface modification mechanisms

A reasonable physical model for the alternative surface-enhanced absorption mechanism was proposed by Iwata et al. [24]. According to this model, the existence of a very thin absorbing layer located at the surface of the wafer can be considered. Very thin layers cannot be detected by conventional absorption measurement techniques. Enhanced optical absorption results from near-surface structural modifications caused, e.g., by chemo-mechanical surface processing during wafer preparation (cutting, grinding, polishing) and consequently the reduced mechanical integrity of the material. Microscopic and nanoscopic sites featuring dangling bonds, native oxide layers, and various lattice defects can initiate the absorption process within the layer. These sites can absorb light with the photon energy below the band gap.

This model is supported by experimental observations of the surface modification morphology. Isolated random micro-damage zones are present in both materials in the focal region, when the laser intensity is close to the threshold. With the increasing number of laser pulses applied, these zones occupy larger surface areas. Therefore, accumulation of laser-induced microscopic defects is one of the driving mechanisms leading to surface modifications observed in the experiments. Light absorption is considerably enhanced by these defects, which provides additional charge carriers for the subsequent avalanche ionization and thermal modification processes.

5.4 Dependence of modification processes on environmental conditions

It is important to note that semiconductors' response to laser irradiation can be considerably affected by variations of environmental conditions, especially the material temperature. For instance, the energy band gap of semiconductors decreases with the increasing temperature. According to the commonly used Varshni relation [28], the temperature dependency of the energy band gap E_g(T) can be approximated by

$$E_g(T) = E_g(0) - \frac{\alpha T^2}{T + \beta}, \tag{4}$$

where α=4.73·10^{-4} eV/K, β=636 K for Si (α=5.41·10^{-4} eV/K, β=204 K for GaAs), and E_g(0) represents the material's band gap energy at T=0 K. This effect can give rise to more favorable conditions for absorption at defect sites with increasing material temperature. Moreover, when the temperature of GaAs reaches approx. 420 °C, the decreased E_g makes two-photon absorption possible. However, the 2PA coefficient is generally small at the corresponding energy threshold, and thus, the contribution of the two-photon absorption in GaAs can be considered unimportant in these experiments.

Elevated material temperature causes changes in electronic and lattice heat conduction parameters of Si and GaAs. In general, the total conductivity and the mobility of electrons and holes decrease with temperature. High laser-induced charge carrier densities lead to further mobility reductions due to electron-hole scattering [18]. On the one hand, these effects can contribute to a more localized energy deposition leading to surface modification through melting and solidification. On the other hand, high pressures can be generated in the bulk material enabling non-equilibrium phase transitions and defects generation, e.g., voids and nano-/micro-cracks. In addition, surface reflectivity increases with temperature (approx. $\Delta R \approx 0.2$ % per ΔT=100 K) [29], which can potentially alter optical energy distribution in the material and surface modification behavior.

In addition, variations of ambient conditions can cause significant differences in laser processing results. For instance, variation of the ambient gas composition and pressure can affect the formation and characteristics of laser-induced plasma, the material removal behavior and rate, the morphology of surface and volume modifications, and support or suppress reactions of the modified material with the environment, e.g., corrosion and oxidation [30]. The use of liquid environments such as water, alcohols, and various aqueous solutions is also well known to influence laser processing [31]. In the present work, all experiments were performed in normal ambient conditions.

Further experimental investigations and modeling are needed to develop a thorough understanding of the underlying fundamental mechanisms resulting in trans-wafer processing of semiconductors, as well as the effects of the process parameters on the processing results.

6 Processing of coated semiconductor surfaces

Utilizing the process knowledge obtained, trans-wafer processing method was applied to the removal of single- and multi-material (metallization) coatings deposited on p-Si wafers featuring base resistivity levels of 4 Ω cm. Unlike intrinsic semiconductors, the p-doped substrates reveal equilibrium charge carriers possibly resulting in linear absorption of laser energy. However, previous research has shown that the aforementioned resistivity level is high enough, so that no substantial absorption occurs [1, 2]. For the experiments, the removal of metallization layers was first studied for the front (laser

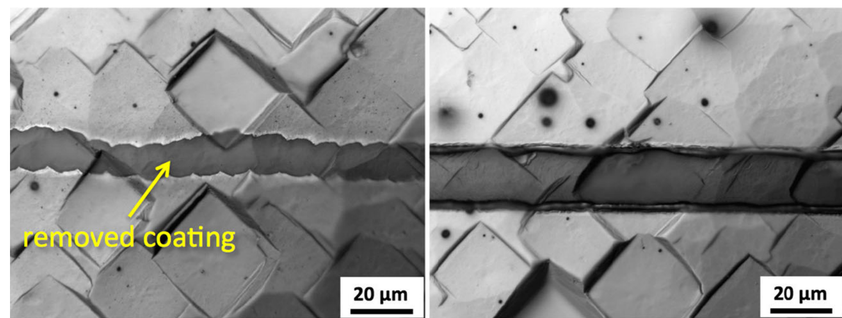

Fig. 8 Examples of metallization removal from the front surface of ML 3 samples. Modifications were produced at the pulse energy E_p=3 µJ (*left*) and E_p=8 µJ (*right*)

incident) surfaces, in order to find out process conditions for selective coating ablation without damaging the substrate. Figure 8 shows examples of metallization removal from the front surface of the sample ML 3. Depending on the process conditions, the combined TiN/Ti layers were successfully removed from the surface without causing visible substrate damage. The minimum laser fluence needed to completely remove the layers was F_{thr}<1.6 J/cm^3. The resistance of the processed sample measured for 10-mm-long modifications (full separation of a metallization layer in two separate portions) was R>76 kΩ.

In the following series of experiments, trans-wafer processing was utilized to remove various material layers form the back surface of Si wafers (Fig. 9). The focus position was chosen to compensate for light refraction in the wafer, according to the thickness of the wafer adopted. Compared to front surface processing, the removal of the back surface metallization produced less consistent surface modifications. At low pulse energies, the processed areas were still partially covered with coating residues. With increasing pulse energy, a gradual disintegration and removal of the coating from the surface was observed. Significant differences in modification behavior were also observed for different thicknesses of the coatings. The consistent removal of thick coatings (ML 4 samples) was not possible without partially damaging the substrate with the process conditions adopted (Fig. 9b, d), whereas processing of thin layers (ML 1 samples) within well-defined modification boundaries was enabled.

In order to study the electrical properties of the separated metallization films, a series of experiments was performed using ML 3 samples (4×25 mm^2) and by processing the samples at different pulse energies in single passes across the width and leaving approx. 1 mm distance between the individual lines. Then the electrical resistance between the separated portions was measured using the 4-terminal method (Fig. 10). The measurements were performed on 4 samples prepared using the same process conditions, and each resistance value was measured at three different locations along the corresponding separation line induced on the metallization layer.

Metallization removal from back surfaces of Si wafers in multiple overlapping tracks was adopted to enable large-area processing (Fig. 11). The distance between the adjacent tracks (track overlap) was varied to achieve processing with a

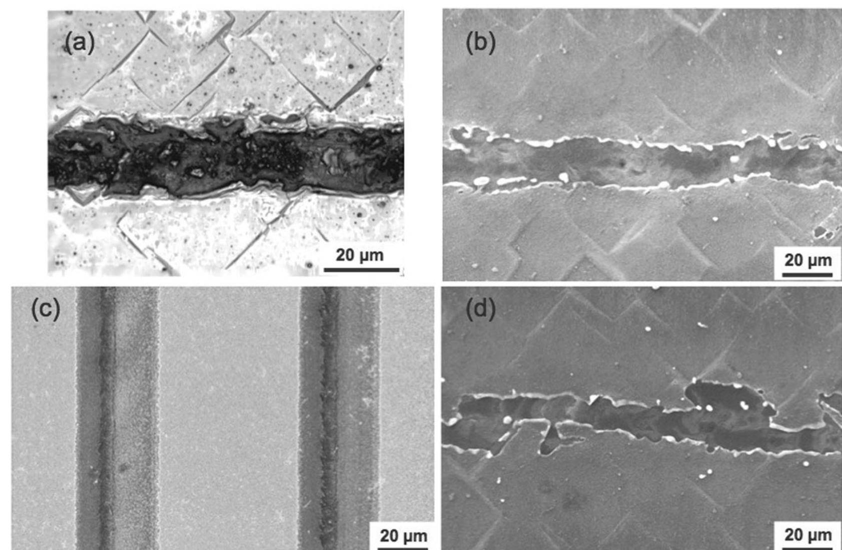

Fig. 9 Examples of trans-wafer metallization removal. **a** ML 3 processed at E_p=35 µJ, **b** ML 4 processed at E_p=32 µJ, **c** ML 1 processed at E_p=35 µJ, and **d** ML4 processed at E_p=22 µJ

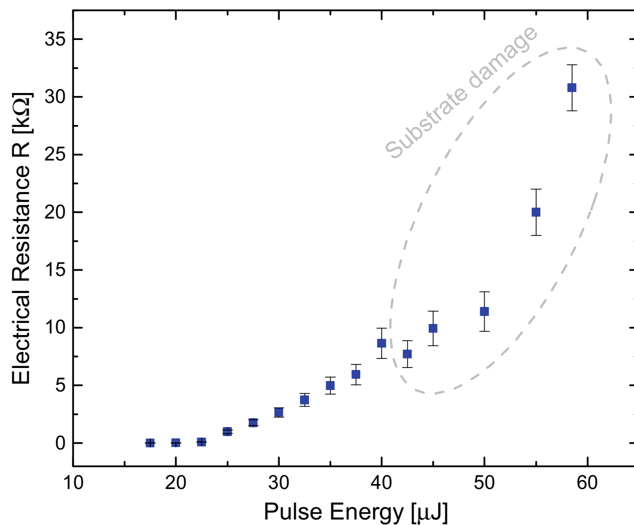

Fig. 10 Electrical resistance of the separated metallization layer in dependence on the laser pulse energy

minimum of debris left. Because the surfaces of the wet-etched samples (ML 3 and 4) exhibited a pyramid pattern, a complete removal of the metallization layers was not possible even at large track overlaps >90 %. Processing of the Ti-coated polished sample (ML 2) however produced large areas free of metallization layer on the order of several mm^2.

7 Other potential application of trans-wafer processing

Based on the experimental results and theoretical considerations presented in this work, a number of various useful applications in semiconductor and microelectronics industry could result from the use of the trans-wafer processing method. Besides layer separation, this method could be potentially adopted to space-selectively modify the resistivity of thin polycrystalline silicon films buried under multi-material semiconductor layers. Previous research on polysilicon thin-film resistors has shown that a resistivity change is caused by the localized crystallization due to laser irradiation [6].

Trans-wafer processing is expected to be a practical method to produce novel material phases in three-dimensional patterns. Recent experiments have shown that such phases could be produced at Si/SiO_2 interfaces by confined micro-explosions caused by high-intensity laser pulses [7].

Finally, trans-wafer melting of semiconductor layers could be potentially adopted, e.g., for alloying of silicon into various metal alloys [8] and localized laser-induced doping of semiconductors [9].

8 Conclusion

In summary, an extensive experimental study was performed to investigate trans-wafer processing of coated and uncoated semiconductor wafers utilizing nanosecond-pulsed laser radiation at the wavelength 2 μm. In order to obtain a thorough process understanding of the physical processes involved, process modeling and simulations were carried out. Laser-induced surface modifications were induced both at the laser incident, at the front surface, and at the back surface of intrinsic Si and GaAs wafers. Consistent modifications of the back surfaces were only possible in trenches, as opposed to irradiation at fixed positions, indicating that surface damage initiation effects could play an important role. Modification thresholds were determined for Si and GaAs at the front and the back surface for different pulse durations, taking into account optical refraction and spatial energy distribution in the wafer. The effective back surface modification thresholds were determined to $F_{thr}<3.2$ J/cm^2 and $F_{thr}<17.2$ J/cm^2 for GaAs and Si, respectively. Intensity-dependent transmission measurements (z-scan) and basic analytic models of the laser-induced semiconductor heating revealed that multi-photon absorption and surface-enhanced absorption at nano- and microscopic defect sites are assumed the main physical mechanisms providing seed charge carriers for subsequent material ionization through secondary processes such as avalanche ionization. Damage accumulation observed in experiments is accountable for consistent surface modifications. Metallization removal was studied for Si wafers featuring different metallization layers. Successful removal resulting in a significant

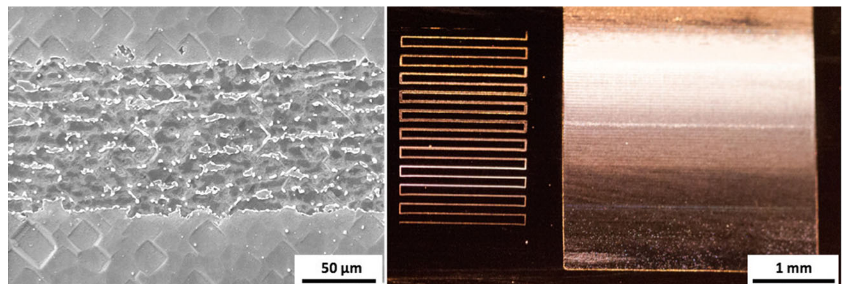

Fig. 11 Examples of large-area metallization removal from back surfaces of Si wafers. Sample ML 4 processed at E_p≈32 μJ (*left*). Sample ML 2 processed at E_p≈ 150 μJ and using an f=25 mm triplet lens (*right*)

increase of electrical resistance was demonstrated. Large-area (multi-mm^2) removal of metallization layers was demonstrated. Further experimental and modeling studies will be needed to obtain a better understanding of the physical phenomena involved in nanosecond laser processing of semiconductors with photon energies smaller than the energy band gap.

Acknowledgments The authors would like to thank Dr. Eric Van Stryland for fruitful discussions and valuable suggestions, as well as Dipl.-Phys. Andreas Brand for providing multi-layer coated Si samples. The authors also acknowledge the support of the Joint Technology Office multidisciplinary research initiative (contract # FA9550-10-1-0543), the Office of Naval Research (contract # N000141210144), the State of Florida, the Fraunhofer-Townes Collaboration, and the NKT Photonics A/S.

References

1. Kumagai M, Uchiyama N, Ohmura E, Sugiura R, Atsumi K, Fukumitsu K (2007) Advanced dicing technology for semiconductor wafer—stealth dicing. IEEE Trans Semicond Manuf 20(3):259–265
2. Ohmura E, Fukuyo F, Fukumitsu K, Morita H (2006) Internal modified-layer formation mechanism into silicon with nanosecond laser. J Achiev Mater Manuf Eng 17(1-2):381–384
3. Bärsch N, Körber K, Ostendorf A, Tönshoff KH (2003) Ablation and cutting of planar silicon devices using femtosecond laser pulses. Appl Phys A 77:237–242
4. Zorba V, Boukos N, Zergioti I, Fotakis C (2008) Ultraviolet femtosecond, picosecond and nanosecond laser microstructuring of silicon: structural and optical properties. Appl Opt 47(11):1846–1850
5. Brown WL (1983) Laser processing of semiconductors. In: Bass M (ed) Laser materials processing. Elsevier, vol. 3, pp. 337–406
6. Boulais E, Fantoni J, Chateauneuf A, Savaria Y, Meunier M (2011) Laser-induced resistance fine tuning of integrated polysilicon thin-film resistors. IEEE Trans Electron Devices 58(2):572–575
7. Rapp L, Haberl B, Bradby JE, Gamaly EG, Williams JS, Rode AV (2014) Confined micro-explosion induced by ultrashort laser pulse at SiO_2/Si interface. Appl Phys A 114:33–43
8. Xu Z, Leong KH, Sanders PG (2000) Laser surface alloying of silicon into aluminum casting alloys. J Laser Appl 12(4):160–170
9. Meseth M, Kunert BC, Bitzer L, Kunze F, Meyer S, Kiefer F, Dehnen M, Orthner H, Petermann N, Kummer M, Wiggers H, Harder N-P, Benson N, Schmechel R (2013) Excimer laser doping using highly doped silicon nanoparticles. Phys Status Solidi A 210(11):2456–2462
10. Wang X, Shen ZH, Lu J, Ni XW (2010) Laser-induced damage threshold of silicon in millisecond, nanosecond, and picosecond regimes. J Appl Phys 108:033103
11. Kuanr AV, Bansal SK, Srivastava GP (1996) Laser induced damage in GaAs at 1.06 μm wavelength: surface effects. Opt Laser Technol 28(1):25–34
12. Lynn Smith J (1972) Surface damage of GaAs from 0.694 and 1.06 laser radiation. J Appl Phys 43:3399
13. Qi H, Wang Q, Zhang X, Liu Z, Zhang S, Chang J (2011) Theoretical and experimental study of laser induced damage on GaAs by nanosecond pulsed irradiation. Opt Lasers Eng 49:285–291
14. Hendow ST, Shakir SA (2010) Structuring materials with nanosecond laser pulses. Opt Express 18(10):10188
15. Garg A, Kapoor A, Tripathi KN (2003) Laser-induced damage studies in GaAs. Opt Laser Technol 35:21–24
16. Parsi Sreenivas VV, Bülters M, Bergmann RB (2012) Microsized subsurface modification of mono-crystalline silicon via non-linear absorption. J Eur Opt Soc Rapid Publ 7:12035
17. Nejadmalayeri AH, Herman PR, Burghoff J, Will M, Nolte S, Tünnermann A (2005) Inscription of optical waveguides in crystalline silicon by mid-infrared femtosecond laser pulses. Opt Lett 30:964
18. Verburg PC, Römer GRBE, Huis in 't Veld AJ (2014) Two-photon-induced internal modification of silicon by erbium-doped fiber laser. Opt Express 22(18):21958–21971
19. Modsching N, Kadwani P, Sims RA, Leick L, Broeng J, Shah L, Richardson M (2011) Lasing in thulium-doped polarizing photonic crystal fiber. Opt Lett 36:3873
20. Kadwani P, Jollivet C, Sims RA, Schülzgen A, Shah L, Richardson M (2012) Comparison of higher-order mode suppression and Q-switched laser performance in thulium-doped large mode area and photonic crystal fibers. Opt Express 20(22):24295–24303K
21. Stutzki F, Jansen F, Jauregui C, Limpert J, Tünnermann A (2013) 2.4 mJ, "33 W Q-switched Tm-doped fiber laser with near diffraction-limited beam quality". Opt Lett 38:99
22. Gaida C, Gebhardt M, Kadwani P, Leick L, Broeng J, Shah L, Richardson M (2013) Amplification of nanosecond pulses to megawatt peak power levels in $Tm3^+$-doped photonic crystal fiber rod. Opt Lett 38:691
23. Liu JM (1982) Simple technique for measurements of pulsed Gaussian-beam spot sizes. Opt Lett 7:196
24. Iwata H, Asakawa K (2008) Accumulative damage of GaAs and InP surfaces induced by multiple-laser-pulse irradiation. Jap J Appl Phys 47(4):2161–2167
25. Meyer JR, Bartoli FJ, Kruer MR (1980) Optical heating in semiconductors. Phys Rev B 21(4):1559–1568
26. Bristow AD, Rotenberg N, van Driel HM (2007) Two-photon absorption and Kerr coefficients of silicon for 850–2200 nm. Appl Phys Lett 90:191104
27. Hurlbut WC, Lee Y-S, Vodopyanov KL, Kuo PS, Feyer MM (2006) Multi-photon absorption and nonlinear refraction of GaAs in the mid-infrared. Opt Lett 32:668
28. Varshni YP (1967) Temperature dependence of the energy gap in semiconductors. Physica 34(1):149–154
29. Jellison GE, Burke HH (1986) The temperature dependence of the refractive index of silicon at elevated temperatures at several laser wavelengths. J Appl Phys 60:841–843
30. Klotzbach U, Mälzer S, Kuntze T, Panzner M, Dötschel M, Sonntag F, Beyer E (2004) Influence of gas on cutting silicon with solid state laser. Proc SPIE 5339:488–493
31. Kruusing A (2010) Handbook of liquids-assisted laser processing. Elsevier